9

Implicit Surface-Based Reconstructions

In surface reconstruction, if the input point cloud is noisy, a surface fitting through the points can be too bumpy for practical use. A remedy to this problem is to define a target smooth implicit surface and project or generate points on this implicit surface for reconstruction. Of course, the main problem is to choose a suitable implicit surface that resembles the original surface which the input point cloud presumably sampled. This means we should prove that the chosen implicit surface is homeomorphic (isotopic) to the sampled surface and is also geometrically close to it. First, we outline a generic approach to achieve this and then specialize the approach to a specific type of implicit surface called MLS surface.

9.1 Generic Approach

Suppose $\mathcal{N} : \mathbb{R}^3 \to \mathbb{R}$ is an implicit function whose zero-level set $\mathcal{N}^{-1}(0)$ is of interest for approximating the sampled surface Σ. The gradient of $\mathcal{N}$ at x is

$$\nabla\mathcal{N}(x) = \left(\frac{\partial\mathcal{N}}{\partial x_1}(x) \;\; \frac{\partial\mathcal{N}}{\partial x_2}(x) \;\; \frac{\partial\mathcal{N}}{\partial x_3}(x)\right).$$

As before let $\Sigma \subset \mathbb{R}^3$ be a compact, smooth surface without boundary. For simplicity assume that Σ has a single connected component. As in previous chapters Ω_O denotes the unbounded component of $\mathbb{R}^3 \setminus \Sigma$ and Ω_I denotes $\mathbb{R}^3 \setminus \Omega_O$. For a point $z \in \Sigma$, $\mathbf{n}_z$ denotes the oriented normal of Σ at z where $\mathbf{n}_z$ points locally toward the unbounded component Ω_O. Let M be the medial axis of Σ.

The entire set $\mathcal{N}^{-1}(0)$ may not approximate Σ. Instead, only the subset of $\mathcal{N}^{-1}(0)$ close to Σ will be the implicit surface of our interest. For this we define a thickening of Σ.

Recall that, for a point $x \in \mathbb{R}^3 \setminus M$, $\tilde{x}$ denotes its closest point in Σ. Let $\phi(x)$ denote the signed distance of a point x to Σ, that is, $\phi(x) = (x - \tilde{x})^T \mathbf{n}_{\tilde{x}}$. For a

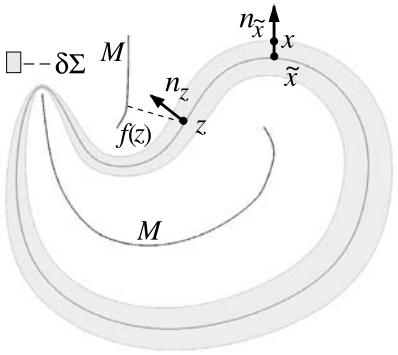

Figure 9.1. The set $\delta\Sigma$, medial axis, and normals.

real $\delta \geq 0$, define offset surfaces $\Sigma_{+\delta}$ and $\Sigma_{-\delta}$ where

$$\Sigma_{+\delta} = \{x \in \mathbb{R}^3 \,|\, \phi(x) = +\delta f(\tilde{x})\}$$

$$\Sigma_{-\delta} = \{x \in \mathbb{R}^3 \,|\, \phi(x) = -\delta f(\tilde{x})\}.$$

Let $\delta\Sigma$ be the region between $\Sigma_{-\delta}$ and $\Sigma_{+\delta}$, that is,

$$\delta\Sigma = \{x \in \mathbb{R}^3 \mid -\delta f(\tilde{x}) \leq \phi(x) \leq \delta f(\tilde{x})\}.$$

Figure 9.1 illustrates the above concepts.

We want to focus on the subset of the zero-level set $\mathcal{N}^{-1}(0)$ near Σ. So, we define $W = \mathcal{N}^{-1}(0) \cap \delta\Sigma$ for a small $\delta > 0$. The proofs of topological equivalence and geometric approximation between W and Σ use two key properties of $\mathcal{N}$.

9.1.1 Implicit Function Properties

HAUSDORFF PROPERTY. We say that $\mathcal{N}$ has the Hausdorff property for δ and δ' if $\delta' < \delta$ and

$$\begin{aligned} \mathcal{N}(x) > 0 \quad & \text{when } x \in (\delta\Sigma \setminus \delta'\Sigma) \cap \Omega_O \\ < 0 \quad & \text{when } x \in (\delta\Sigma \setminus \delta'\Sigma) \cap \Omega_I. \end{aligned}$$

The above inequalities mean that $\mathcal{N}(x)$ crosses zero value in $\delta\Sigma$ only when x is in $\delta'\Sigma$. This implies that $\mathcal{N}^{-1}(0) \cap \delta\Sigma$ indeed resides in $\delta'\Sigma$.

GRADIENT PROPERTY. Let z be any point in Σ. Let $\ell_{\mathbf{n}_z}$ be the oriented line containing the normal $\mathbf{n}_z$ to Σ at z. Let $[\mathbf{u}]\mathcal{N}(x)$ be the directional derivative of $\mathcal{N}$ at x along the vector $\mathbf{u}$, that is, $[\mathbf{u}]\mathcal{N}(x)$ is $\mathbf{u}^T \nabla\mathcal{N}(x)$. We say $\mathcal{N}$ has the

gradient property for δ if

$$[\mathbf{n}_z]\mathcal{N}(x) > 0 \quad \text{for any } x \in \ell_{\mathbf{n}_z} \cap \delta\Sigma.$$

The directional derivative $[\mathbf{n}_z]\mathcal{N}(x)$ is the projection of the gradient $\nabla\mathcal{N}(x)$ along $\ell_{\mathbf{n}_z}$. Therefore, the gradient property implies that $\nabla\mathcal{N}(x)$ is not zero in $\delta\Sigma$.

9.1.2 Homeomorphism Proof

We show that if $\mathcal{N}$ has the Hausdorff property for δ and δ', and the gradient property for δ' where $\delta' < \delta < 1$, the subset

$$W = \mathcal{N}^{-1}(0) \cap \delta\Sigma$$

is homeomorphic to Σ. First, observe that Hausdorff property implies W is indeed a subset of $\delta'\Sigma$. Second, the gradient property implies that $\nabla\mathcal{N}$ does not vanish in $\delta'\Sigma$. Therefore, by the implicit function theorem in differential topology, W is a compact, smooth 2-manifold.

Consider the map $\nu : \mathbb{R}^3 \setminus M \to \Sigma$ that takes a point $x \in \mathbb{R}^3$ to its closest point in Σ. We show that ν defines a homeomorphism when restricted to W. Let ν' denote this restriction.

Lemma 9.1. *If $\mathcal{N}$ has the Hausdorff property for δ and δ' where $\delta < 1$, ν' is well defined and surjective.*

Proof. Since $\delta < 1$, W avoids M as all points of W are in $\delta\Sigma$ by definition. Therefore, ν' avoids M and hence is well defined.

Let z be any point in Σ. The normal line $\ell_{\mathbf{n}_z}$, through z along the normal $\mathbf{n}_z$, intersects $\mathcal{N}^{-1}(0)$ within $\delta\Sigma$, thanks to the Hausdorff property. Thus, by definition of W, it intersects W at a point. Therefore, for each point $z \in \Sigma$, there is a point in W which is mapped by ν' to z. ■

Lemma 9.2. *If $\mathcal{N}$ has the Hausdorff property for δ and δ' as well as the gradient property for δ' where $\delta' < \delta < 1$, ν' is injective.*

Proof. To prove the injectivity of ν', assume for the sake of contradiction that there are two points w and w' in W so that $\nu'(w) = \nu'(w') = z$. This means $\ell_{\mathbf{n}_z}$ intersects W at w and w' within $\delta'\Sigma$ (Hausdorff property). Without loss of generality assume that w and w' are two such consecutive intersection points. It follows that the oriented line $\ell_{\mathbf{n}_z}$ makes at least $\frac{\pi}{2}$ angle with one of the normals

to W at w and w'. But, that is impossible since the gradient property implies that

$$\angle(\mathbf{n}_z, \nabla\mathcal{N}(x)) < \frac{\pi}{2}$$

for any point $x \in \ell_{\mathbf{n}_z} \cap \delta'\Sigma$. ■

Theorem 9.1. *If $\mathcal{N}$ has the Hausdorff property for δ and δ' as well as the gradient property for δ' where $\delta' < \delta < 1$, ν' is a homeomorphism.*

Proof. The function ν' is continuous since ν is. Since W is compact, it is sufficient to establish that ν' is surjective and injective which are the statements of Lemma 9.1 and Lemma 9.2 respectively. ■

Several implicit surfaces have been proposed with different algorithms for their computations in the literature. Among them we focus on the class of surfaces defined by a technique called *moving least squares*. These surfaces, generically, are called MLS surfaces.

9.2 MLS Surfaces

Our goal is to formulate an implicit surface that fits the input points well. In particular, we would like to prove the Hausdorff and the gradient property for the implicit function that defines the implicit surface. *Least squares* is a numerical technique developed to fit a function to a given input data. Let a function $\Phi : \mathbb{R}^3 \to \mathbb{R}$ be sampled at the points in $P \subset \mathbb{R}^3$. This means each point $p \in P$ has an associated function value $\phi_p = \Phi(p)$. Suppose we wish to design an implicit function $\mathcal{I} : \mathbb{R}^3 \to \mathbb{R}$ that fits the data points as close as possible with respect to some metric. If this metric is the sum of the squares of the errors at the data points, we get the well-known least squares solution. Specifically, we minimize the error

$$\Sigma_{p\in P}(\mathcal{I}(p) - \phi_p)^2 \tag{9.1}$$

to obtain a solution for $\mathcal{I}$. In our case we would like the implicit surface given by $\mathcal{I}^{-1}(0)$ to fit the given input points P. We modify the basic least squares technique as follows. First, each function value ϕ_p is replaced with a function $\phi_p : \mathbb{R}^3 \to \mathbb{R}$ where $\phi_p(p) = 0$. Then, taking

$$\mathcal{I}(x) = \Sigma_{i=1}^{n} c_i b_i(x) \tag{9.2}$$

where c_i is the coefficient for the ith basis function $b_i(x)$, one can minimize

$$\Sigma_{p\in P}(\mathcal{I}(x) - \phi_p(x))^2 \tag{9.3}$$

over the unknown coefficients. The intention here is that the resulting solution $\mathcal{I}$ fits each function $\phi_p(x)$ well and in particular when x is near p. Since $\phi_p(p) = 0$, this would mean that the implicit surface given by $\mathcal{I}^{-1}(0)$ fits the points in P. However, this does not happen in general as the least square fit given by the minimization of the expression in 9.3 does not give any preference to $\phi_p(x)$ when x is near p. We achieve this goal by weighting the contributions of the errors differently. We use a weight function $\theta_p : \mathbb{R}^3 \to \mathbb{R}$ for the point p so that it takes a larger value than all other weight functions when x is near p. So, we minimize

$$\Sigma_{p \in P}(\mathcal{I}(x) - \phi_p(x))^2 \theta_p(x).$$

The effects of the weights make the least square fit change or "move" which lead to the terminology *moving least squares* or MLS in short for the resulting implicit surface.

For simplicity we choose $\mathcal{I}(x) = c_0$ letting all other $c_i = 0$ in Equation 9.2. Notice that c_0 will be a function of x instead of a constant. The minimization leads to the equation

$$\Sigma_{p \in P} 2(c_0 - \phi_p(x))\theta_p(x) = 0$$
$$\text{or, } \mathcal{I}(x) = c_0 = \frac{\Sigma_{p \in P} \phi_p(x)\theta_p(x)}{\Sigma_{p \in P} \theta_p(x)}.$$

We would like the implicit surface $\mathcal{I}^{-1}(0)$ not only match the sampled surface in Hausdorff distance but also match its normals. So, we assume that each sample point is equipped with an estimated normal. Let $\mathbf{v}_p$ denote the assigned normal to the sample point p. Then, the gradient $\nabla\mathcal{I}(p)$ should approximate $\mathbf{v}_p$. Keeping this in mind we choose

$$\phi_p(x) = (x - p)^T \mathbf{v}_p.$$

With these choices the MLS surface is the zero-level set of

$$\mathcal{I}(x) = \frac{\Sigma_{p \in P}((x - p)^T \mathbf{v}_p)\theta_p(x)}{\Sigma_{p \in P} \theta_p(x)}. \tag{9.4}$$

9.2.1 Adaptive MLS Surfaces

Weighting Functions

The implicit function value $\mathcal{I}(x)$ at a point x should be primarily decided by the nearby sample points. That is exactly the reason why the MLS function weighs the sample points differently in a sum instead of giving them equal weights. We will adopt the noise model as in Chapter 8, that is, a $(\varepsilon, \varepsilon^2, -)$-

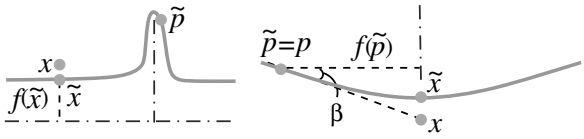

Figure 9.2. The solid curves and the dash–dot lines represent part of the surface and its medial axis respectively.

sample for a suitably small $\varepsilon > 0$. This model implies that the sample points within a sufficiently small neighborhood of a point x near Σ are predictably distributed within a small slab (Lemma 9.4). However, the surface Σ and its sample points outside this neighborhood could be arbitrarily distributed. Hence, we should design a weighting function such that the sample points outside the neighborhood have much less effect on the implicit function than those inside.

Our first step to meet the above requirements is to choose Gaussian functions as the weights since their widths can control the influence of the sample points. Therefore, the weighting function $\theta_p(x)$ is chosen as a Gaussian function with a support width h around p, that is,

$$\theta_p(x) = \exp^{\|x-p\|^2/h^2}. \tag{9.5}$$

Essentially, h determines the neighborhood from where the sample points have dominant effects on the implicit function. To make the implicit surface sensitive to features of Σ, one may take h to be a fraction of the local feature size. However, one needs to be more careful. If we simply take a fraction of $f(\tilde{x})$ as the width, that is, take $\exp^{-\frac{\|x-p\|^2}{[\rho f(\tilde{x})]^2}}$ as the weighting function for some $\rho < 1$, we cannot bound the effect of the far away sample points. Consider the left picture in Figure 9.2. The local feature size at the point $\tilde{p}$ can be arbitrarily small requiring the number of sample points around $\tilde{p}$ to be arbitrarily large to meet the sampling conditions. Consequently, the summation of the weights over those sample points which are outside $B_{x,f(\tilde{x})}$ becomes too large to be dominated by the contributions of the sample points in the neighborhood $B_{x,f(\tilde{x})}$ of x.

An alternative option is to take a fraction of $f(\tilde{p})$ as the width, that is, take $\exp^{-\frac{\|x-p\|^2}{[\rho f(\tilde{p})]^2}}$ as the weighting function. However, it also fails as illustrated in the right picture in Figure 9.2. The sample points such as p has a constant weight $\exp^{-\frac{1}{[\rho\cos\beta]^2}}$. As the summation extends outside the neighborhood of x, the contribution of the sample points remains constant instead of decreasing. As a result, one cannot hope to bound the outside contribution.

We overcome the difficulty by using a combination of the above two options, that is, by taking a fraction of $\sqrt{f(\tilde{x})f(\tilde{p})}$ as the width of the Gaussian

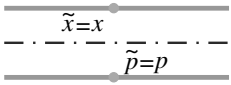

Figure 9.3. The solid and the dash–dot lines represent part of the surface and its medial axis respectively.

weighting functions. This takes into account the effects from both members, the contribution sender p and the contribution receiver x. Unlike $\exp^{-\frac{\|x-p\|^2}{[\rho f(\tilde{p})]^2}}$, such form of weighting function decreases as p goes away from x. In addition, such form of weighting function assigns a small value to the points that sample small features, which in turn cancels out the effect that small features require more sample points.

There is still one more difficulty. The function f, though continuous, is not smooth everywhere on Σ. The nonsmoothness appears where Σ intersects the medial axis of its own medial axis M. To make the implicit function smooth, we use a smooth function σ arbitrarily close to f where

$$|\sigma(x) - f(x)| \leq \beta f(x) \tag{9.6}$$

for arbitrarily small $\beta > 0$. This is doable since the family of real-valued smooth functions over smooth manifolds is dense in the family of continuous functions and the minimal feature size is strictly positive for any manifold that is at least C^2-smooth. Finally, we choose a fraction (given by ρ) of $\sqrt{\sigma(\tilde{x})\sigma(\tilde{p})}$ as the width of the Gaussian weighting functions. Specifically, we take

$$\ln \theta_p(x) = -\frac{\sqrt{2}\|x - p\|^2}{\rho^2 \sigma(\tilde{p})\sigma(\tilde{x})}. \tag{9.7}$$

The factor $\sqrt{2}$ in the exponent is for the convenience in proofs as one may see later. In general, it is known that larger values of ρ make the MLS surface look smoother. To have a sense of appropriate values of ρ, consider the case where x is on the surface Σ. The sample points such as p in Figure 9.3 across the medial axis to point x should have little effect on the implicit function value at x. Taking $\rho \leq 0.4$ makes the weight of p at x less than $\exp^{-25\sqrt{2}} \approx 5 \times 10^{-16}$ since $\|x - p\| \geq 2 \max\{f(\tilde{x}), f(\tilde{p})\}$.

AMLS Function

With the weighting function given by Equation 9.7 we define the implicit function. Since the weights adapt to the local feature size, we call this function *adaptive* MLS or AMLS in short. The implicit surface given by the AMLS

function is referred as AMLS surface. Let

$$\mathcal{N}(x) = \sum_{p \in P}((x - p)^T \mathbf{v}_p)\theta_p(x) \tag{9.8}$$

where θ_p is given by Equation 9.7. The AMLS function is given by

$$\mathcal{I}(x) = \frac{\mathcal{N}(x)}{\mathcal{W}(x)}$$

where

$$\mathcal{W}(x) = \sum_{p \in P} \theta_p(x).$$

Obviously, the implicit functions $\mathcal{N}$ and $\mathcal{I}$ have exactly the same zero-level set, that is, $\mathcal{I}^{-1}(0) = \mathcal{N}^{-1}(0)$. Therefore, we could have taken $\mathcal{N}$ instead of $\mathcal{I}$ for AMLS, but we observe in Section 9.6.3 that $\mathcal{I}$ has a significant computational advantage since Newton iteration for $\mathcal{I}$ has a much larger convergent domain than the one for $\mathcal{N}$. However, the function $\mathcal{N}$ has a simpler form to analyze. Hence, we analyze the zero-level set of $\mathcal{I}$ via the function $\mathcal{N}$.

9.3 Sampling Assumptions and Consequences

Our goal is to establish that the function $\mathcal{N}$ as defined in Equation 9.8 has the Hausdorff and gradient properties. This would require that the input point set P sample Σ densely though possibly with noise. Following the definition of noisy sample in Chapter 7 we assume that the input P is a $(\varepsilon, \varepsilon^2, \kappa)$-sample of Σ for some $\varepsilon < 1$ and $\kappa \geq 1$. In addition, we assume that each sample point is equipped with a normal with the following condition.

Normal assignment. The normal $\mathbf{v}_p$ assigned to a point $p \in P$ makes an angle of at most ε with the normal $\mathbf{n}_{\tilde{p}}$ at its closest point $\tilde{p}$ on Σ.

The sampling assumptions lead to the following result which would be used in our analysis.

Lemma 9.3. *For $\varepsilon < 0.01$ and any $x \in \mathbb{R}^3$, the number of sample points inside a ball $B_{x, \frac{\varepsilon}{2} f(\tilde{x})}$ is less than 10κ.*

Proof. Let p be any sample point in $B_{x, \frac{\varepsilon}{2} f(\tilde{x})}$. We have

$$\|x - p\| \leq \frac{\varepsilon}{2} f(\tilde{x})$$

$$\text{or, } \|x - \tilde{p}\| \leq \frac{\varepsilon}{2} f(\tilde{x}) + \varepsilon^2 f(\tilde{p})$$

and

$$\begin{aligned}\|\tilde{x} - \tilde{p}\| &\leq \|x - \tilde{x}\| + \|x - \tilde{p}\| \\ &\leq 2\|x - \tilde{p}\| \\ &\leq \varepsilon f(\tilde{x}) + 2\varepsilon^2 f(\tilde{p}). \end{aligned} \tag{9.9}$$

From the Lipschitz property of f and Inequality 9.9 we get

$$\frac{1-\varepsilon}{1+2\varepsilon^2} f(\tilde{x}) \leq f(\tilde{p}) \leq \frac{1+\varepsilon}{1-2\varepsilon^2} f(\tilde{x}). \tag{9.10}$$

By sampling condition the ball $B = B_{p,\varepsilon f(\tilde{p})}$ contains at most κ sample points. Thus, B can count for at most κ sample points in $B_{x,\frac{\varepsilon}{2} f(\tilde{x})}$. To count other sample points we can take a sample point, say q, outside B and again consider the ball $B_{q,\varepsilon f(\tilde{q})}$. We can continue this process each time choosing a center outside all the balls so far considered till we cover all sample points. We determine an upper bound on the number of such balls that are needed to cover all sample points.

We claim that the center, say p, of such a ball is at least $\varepsilon' f(\tilde{p})$ away from any other center q where

$$\varepsilon' = \frac{\varepsilon(1-\varepsilon-\varepsilon^2)}{1+\varepsilon^2}.$$

If q is introduced after p, we have $\|p - q\| \geq \varepsilon f(\tilde{p})$ which is more than the claimed bound. When p is introduced after q, it is at least $\varepsilon f(\tilde{q})$ away from q. If $\|p - q\| > \varepsilon f(\tilde{p})$ we are done. So, assume $\|p - q\| \leq \varepsilon f(\tilde{p})$. Then,

$$\begin{aligned} f(\tilde{q}) &\geq f(\tilde{p}) - \|\tilde{p} - \tilde{q}\| \\ &\geq f(\tilde{p}) - \|\tilde{p} - p\| - \|p - q\| - \|q - \tilde{q}\| \\ &\geq f(\tilde{p}) - \varepsilon^2 f(\tilde{p}) - \varepsilon f(\tilde{p}) - \varepsilon^2 f(\tilde{q}) \end{aligned}$$

which gives

$$f(\tilde{q}) \geq \frac{(1-\varepsilon-\varepsilon^2)}{1+\varepsilon^2} f(\tilde{p}).$$

Since $\|p - q\| \geq \varepsilon f(\tilde{q})$, the claimed bound is immediate.

So, if we consider balls of half the size, that is, for a center p if we consider a ball of size $\frac{\varepsilon'}{2} f(\tilde{p})$ they will be disjoint. From Inequality 9.10 each such ball has a radius at least

$$r = \frac{\varepsilon'(1-\varepsilon)}{2(1+2\varepsilon^2)} f(\tilde{x}).$$

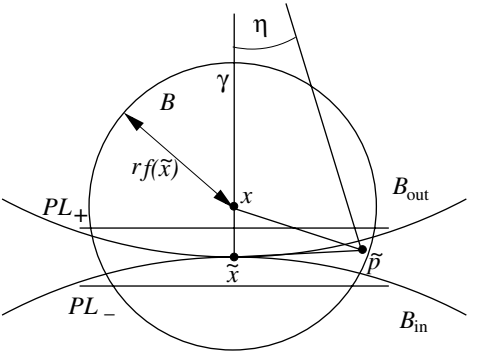

Figure 9.4. Illustration for Lemma 9.4: η is the angle between $\tilde{x}m$ and $\tilde{p}m$ where m is the center of the medial ball.

Also, each such ball will be inside the ball $B' = B_{x,\frac{\varepsilon}{2}f(\tilde{x})+\frac{\varepsilon'}{2}f(\tilde{p})}$. Inequality 9.10 provides that the radius of B' is at most

$$R = \frac{\varepsilon(1-2\varepsilon^2)+\varepsilon'(1+\varepsilon)}{2(1-2\varepsilon^2)} f(\tilde{x}).$$

One can pack at most $\frac{R^3}{r^3}$ balls of radius r inside a ball of radius R. This implies that there are at most $\frac{R^3}{r^3}\kappa$ sample points inside the ball $B_{x,\frac{\varepsilon}{2}f(\tilde{x})}$. We have

$$\begin{aligned}\frac{R^3}{r^3}\kappa &= \left(\frac{(\varepsilon(1-2\varepsilon^2)+\varepsilon'(1+\varepsilon))(1+2\varepsilon^2)}{\varepsilon'(1-2\varepsilon^2)(1-\varepsilon)}\right)^3 \kappa \\ &\leq 10\kappa \text{ for } \varepsilon < 0.01.\end{aligned}$$

■

For our proofs we need a result that all sample points near a point x in a small tubular neighborhood of Σ lie within a small slab centering $\tilde{x}$. Denote $S_{x,r}$ to be the boundary of $B_{x,r}$. Consider any point x on $\Sigma_{+\delta}$ or $\Sigma_{-\delta}$ and a ball $B_{x,rf(\tilde{x})}$ with a small radius $r < 1$. Let PL_+ and PL_- be two planes perpendicular to $\mathbf{n}_{\tilde{x}}$ and at a small distance $\omega f(\tilde{x})$ from $\tilde{x}$ (Figure 9.4). We show that if ω is of the order of $\varepsilon^2 + r^2$, all points of P within the ball $B_{x,rf(\tilde{x})}$ lie within the slab made by PL_+ and PL_-.

Lemma 9.4. *For $\delta < 0.5$ and $\varepsilon < 0.1$, let x be a point on $\Sigma_{+\delta}$ or $\Sigma_{-\delta}$ and p be any sample point inside $B_{x,rf(\tilde{x})}$ where $\delta < r < 1$. Let $R(r) = (\delta + r) + \frac{1+r+\delta}{1-\varepsilon^2}\varepsilon^2$. The following facts hold.*

(i) If $R(r) < \frac{1}{3}$ *then* $\angle(\mathbf{n}_{\tilde{x}}, \mathbf{v}_p) < \frac{R(r)}{1-3R(r)} + \varepsilon$.

(ii) p *lies inside the slab bounded by two planes* PL_+ *and* PL_- *which are perpendicular to* $\mathbf{n}_{\tilde{x}}$ *and at a distance of* $\omega(r) f(\tilde{x})$ *from* $\tilde{x}$ *where* $\omega(r) = \frac{R(r)^2}{2} + \frac{1+r+\delta}{1-\varepsilon^2}\varepsilon^2$.

Proof. Let B be the ball $B_{x, rf(\tilde{x})}$. We have

$$\|\tilde{p} - \tilde{x}\| \leq (\delta + r) f(\tilde{x}) + \varepsilon^2 f(\tilde{p}). \tag{9.11}$$

From Lipschitz property of f, we obtain

$$f(\tilde{p}) \leq \frac{1 + r + \delta}{1 - \varepsilon^2} f(\tilde{x}). \tag{9.12}$$

It follows from Inequalities 9.11 and 9.12 that

$$\|\tilde{x} - \tilde{p}\| \leq R(r) f(\tilde{x}). \tag{9.13}$$

If $R(r) < \frac{1}{3}$, $\angle(\mathbf{n}_{\tilde{x}}, \mathbf{n}_{\tilde{p}}) < \frac{R(r)}{1-3R(r)}$ by the Normal Variation Lemma 3.3 which together with $\angle(\mathbf{n}_{\tilde{p}}, \mathbf{v}_p) < \varepsilon$ shows (i).

Let γ be the radius of either of the two medial balls B_{out} or B_{in} at $\tilde{x}$. Obviously, $\gamma \geq f(\tilde{x})$. Furthermore, we have

$$\sin \frac{\eta}{2} \leq \frac{\|\tilde{x} - \tilde{p}\|}{2\gamma} \tag{9.14}$$

where η is the angle illustrated in Figure 9.4. The distance from $\tilde{p}$ to the tangent plane at $\tilde{x}$ is less than $\gamma(1 - \cos\eta) = 2\gamma \sin^2 \frac{\eta}{2}$. Hence, the distance from p to the tangent plane at $\tilde{x}$ is less than $2\gamma \sin^2 \frac{\eta}{2} + \varepsilon^2 f(\tilde{p})$, which shows (ii) by substituting Inequalities 9.12, 9.13, and 9.14. ■

9.3.1 Influence of Samples

We have formulated the implicit function $\mathcal{I}$ keeping in mind that, for any point $x \in \mathbb{R}^3$, the effect of the distant sample points on $\mathcal{I}(x)$ and hence on $\mathcal{N}(x)$ could be bounded. We establish this result formally in this section. For this result we will need an upper bound on the number of points that can reside inside a small ball $B_{x, \frac{\rho}{2} f(\tilde{x})}$ for some small ρ. Let $\lambda = \lambda(\rho)$ be this number. Notice that we have already derived an upper bound on λ for $\rho = \varepsilon$ in Lemma 9.3. We will use this specific value of ρ later in our proof. At this stage we work without specifying any particular value for ρ and use λ for the number of points inside $B_{x, \frac{\rho}{2} f(\tilde{x})}$.

In various claims, the contribution of a sample point p to the implicit function $\mathcal{N}$ or its derivative at a point x will be bounded from above by an expression

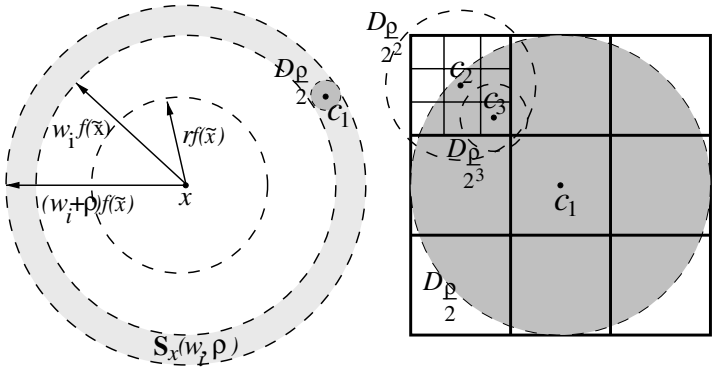

Figure 9.5. The nested shells and the hierarchical subdivision tree.

that involves the term

$$I_p(x) = \exp^{-\frac{\sqrt{2}\|x-p\|^2}{\rho^2\sigma(\tilde{p})\sigma(\tilde{x})}} \cdot \frac{\|x-p\|^s}{[\frac{\rho^2}{\sqrt{2}}\sigma(\tilde{p})\sigma(\tilde{x})]^t}.$$

The values of s and t will vary between 0 to 2 and 0 to 1 respectively in various equations where I_p is used. For instance, the contribution of a sample point p to the function $\mathcal{N}$ at x can be bounded by $I_p(x)$ with $s = 1$ and $t = 0$.

Our strategy for bounding $I_p(x)$ will be to decompose the space into spherical shells centering x. Theorem 9.2 shows that the total contribution from all sample points in the shells decreases as their distances from x increase. Let $\mathbb{S}_x(w, \rho)$ be the shell region between the spheres $S_{x,wf(\tilde{x})}$ and $S_{x,(w+\rho)f(\tilde{x})}$. For $i = 0, 1, \ldots$ consider the nested shells given by $\mathbb{S}_x(w_i, \rho)$ where $w_i = r + i\rho$ (Figure 9.5). To prove Theorem 9.2 we need a result that bounds the total contribution of the sample points lying within the intersection of a small ball of radius $\frac{\rho}{2} f(\tilde{x})$ and the shell $\mathbb{S}_x(w_i, \rho)$. Let $D_{\frac{\rho}{2}}$ be any such ball. We would like to bound the sum $\sum_{p \in D_{\frac{\rho}{2}} \cap \mathbb{S}_x(w_i,\rho)} I_p(x)$. The ball $D_{\frac{\rho}{2}}$ has a radius $\frac{\rho}{2} f(\tilde{x})$ though its center is not necessarily x. Therefore, we cannot use $\lambda = \lambda(\rho)$ to bound the number of sample points inside $D_{\frac{\rho}{2}}$. We overcome this difficulty by using a hierarchical subdivision of the smallest cube NC_1 containing $D_{\frac{\rho}{2}}$. The subdivision divides a cube unless it can be covered with a ball $B_{c,r}$ where r is a fraction of $f(\tilde{c})$. Then, one can use $\lambda = \lambda(\rho)$ to bound the number of sample points in $B_{c,r}$ and hence in the cubes of the subdivision. Therefore, we can bound the number of sample points in $D_{\frac{\rho}{2}}$ using the number of the leaf nodes in its corresponding subdivision tree. Notice that we do not have an explicit bound for the number of sample points in any $D_{\frac{\rho}{2}}$ since at different positions $D_{\frac{\rho}{2}}$ may have different subdivision trees adapting

to the local geometry of the surface. However, we do have an explicit upper bound for the total weights from the sample points inside any $D_{\frac{\rho}{2}}$ as proved in Lemma 9.5.

Assume a hierarchical subdivision tree HST of NC_1 as follows. Let c_1 be the center of the bounding cube NC_1. Subdivide NC_1 into 27 subcubes of size $\frac{\rho}{3} f(\tilde{x})$ if $f(\tilde{c}_1) < f(\tilde{x})$. Let NC_2 be any such subcube. It can be covered by a ball $D_{\frac{\rho}{2^2}} = B_{c_2, \frac{\rho}{2^2} f(\tilde{x})}$ where c_2 is the center of NC_2. Subdivide NC_2 in the same way if $f(\tilde{c}_2) < \frac{1}{2} f(\tilde{x})$. In general, keep subdividing a subcube NC_k at the kth level if $f(\tilde{c}_k) < \frac{1}{2^{k-1}} f(\tilde{x})$ where c_k is the center of NC_k. Observe that NC_k is covered by $D_{\frac{\rho}{2^k}} = B_{c_k, \frac{\rho}{2^k} f(\tilde{x})}$. Figure 9.5 shows an HST in two dimensions. We use NC_k to also denote its intersection with $D_{\frac{\rho}{2^k}}$.

Lemma 9.5. *If $\rho \leq 0.4$, $\varepsilon \leq 0.1$, and $r \geq 5\rho$, then*

$$\sum_{p \in D_{\frac{\rho}{2}} \cap \mathbb{S}_x(w_i, \rho)} I_p(x) \leq \lambda \exp^{-\frac{r w_i}{(1+2r)\rho^2}} \cdot \frac{w_i^s}{\rho^{2t}} \sigma(\tilde{x})^{s-2t}$$

where $0 \leq s \leq 2$, $0 \leq t \leq 1$, $w_i = r + i\rho$ and λ is defined earlier.

Proof. Case 1: $f(\tilde{c}_1) \geq f(\tilde{x})$: HST has only one node NC_1. Let p be any sample point in $D_{\frac{\rho}{2}}$. Observe that $\|\tilde{p} - \tilde{c}_1\| \leq 2\|\tilde{p} - c_1\| \leq 2(\|\tilde{p} - p\| + \|p - c_1\|) \leq 2\varepsilon^2 f(\tilde{p}) + \rho f(\tilde{c_1})$. By Lipschitz property of f,

$$f(\tilde{p}) \geq \frac{1-\rho}{1+2\varepsilon^2} f(\tilde{x}).$$

From Inequality 9.6 we have

$$\sigma(\tilde{p}) \geq \frac{1-\rho}{\beta'(1+2\varepsilon^2)} \sigma(\tilde{x})$$

where $\beta' = \frac{1+\beta}{1-\beta}$. Similarly, from condition $\|x - p\| \geq r f(\tilde{x})$ (p lies in $\mathbb{S}_x(w_i, \rho)$) and the fact $\|\tilde{x} - \tilde{p}\| \leq 2(\|x - p\| + \|p - \tilde{p}\|) \leq 2\|x - p\| + 2\varepsilon^2 f(\tilde{p})$ we obtain

$$\sigma(\tilde{p}) \leq (1+\beta) \frac{1+2r}{r(1-2\varepsilon^2)} \|x - p\|.$$

Hence,

$$I_p(x) \leq \exp^{-\frac{\sqrt{2}(1-2\varepsilon^2)}{(1+\beta)(1+2r)} \frac{r\|x-p\|}{\rho^2 \sigma(\tilde{x})}} \cdot \left[\frac{\sqrt{2}\beta'(1+2\varepsilon^2)}{1-\rho} \right]^t \cdot \frac{\|x - p\|^s}{[\rho\sigma(\tilde{x})]^{2t}}$$

which is a decreasing function of $\|x-p\|$ when $\|x-p\| \geq 4\rho\sigma(\tilde{x})$. Since $\|x-p\| \geq \frac{w_i\sigma(\tilde{x})}{1+\beta}$, we have

$$\begin{aligned} I_p(x) &\leq \exp^{-\frac{\sqrt{2}(1-2\varepsilon^2)}{(1+\beta)^2(1+2r)}\frac{rw_i}{\rho^2}} \cdot \frac{[\sqrt{2}\beta'(1+2\varepsilon^2)]^t}{(1-\rho)^t(1+\beta)^s} \cdot \frac{w_i^s}{\rho^{2t}}\sigma(\tilde{x})^{s-2t} \\ &\leq \exp^{-\frac{rw_i}{(1+2r)\rho^2}} \cdot \frac{w_i^s}{\rho^{2t}}\sigma(\tilde{x})^{s-2t}. \end{aligned}$$

It is not hard to verify the second inequality under the given conditions. The lemma follows from the fact that $B_{c_1,\frac{\rho}{2}f(\tilde{c}_1)}$ covers $D_{\frac{\rho}{2}}$ and hence the number of sample points inside $D_{\frac{\rho}{2}}$ is less than λ.

Case 2: $f(\tilde{c}_1) < f(\tilde{x})$: Consider a leaf node NC_k at the kth level which is covered by $D_{\frac{\rho}{2^k}}$ in HST. We have $f(\tilde{c}_k) \geq \frac{1}{2^{k-1}}f(\tilde{x})$. Let p be any sample point inside the node. Since $\|\tilde{p}-\tilde{c}_k\| \leq 2\|\tilde{p}-c_k\|$, we obtain

$$\sigma(\tilde{p}) \geq \frac{1-\rho}{\beta'(1+2\varepsilon^2)} \cdot \frac{1}{2^{k-1}}\sigma(\tilde{x}).$$

On the other hand, p is also inside the parent node NC_{k-1} covered by $D_{\frac{\rho}{2^{k-1}}}$ in HST. Since $\|\tilde{p}-\tilde{c}_{k-1}\| \leq 2\|\tilde{p}-c_{k-1}\|$ and $f(\tilde{c}_{k-1}) < \frac{1}{2^{k-2}}f(\tilde{x})$, we obtain

$$\sigma(\tilde{p}) \leq \frac{\beta'(1+\rho)}{1-2\varepsilon^2} \cdot \frac{1}{2^{k-2}}\sigma(\tilde{x}).$$

Hence, for the given value of ρ and ε, we have

$$\begin{aligned} &I_p(x) \\ &\leq \exp^{-2^{k-2}\frac{\sqrt{2}(1-2\varepsilon^2)}{\beta'(1+\rho)}\frac{\|x-p\|^2}{[\rho\sigma(\tilde{x})]^2}} \cdot 2^{t(k-2)}\left[\frac{2\sqrt{2}\beta'(1+2\varepsilon^2)}{1-\rho}\right]^t \cdot \frac{\|x-p\|^s}{[\rho\sigma(\tilde{x})]^{2t}} \\ &\leq \frac{1}{27}\exp^{-2^{k-2}\frac{rw_i}{(1+2r)\rho^2}} \cdot 2^{t(k-2)} \cdot \frac{w_i^s}{\rho^{2t}}\sigma(\tilde{x})^{s-2t}. \end{aligned}$$

Since $B_{c_k,\frac{\rho}{2}f(\tilde{c}_k)}$ covers $D_{\frac{\rho}{2^k}}$ and hence the number of sample points inside the leaf node NC_k is less than λ, we have

$$\sum_{p\in NC_k} I_p(x) \leq \frac{1}{27} \cdot \lambda \exp^{-2^{k-2}\frac{rw_i}{(1+2r)\rho^2}} \cdot 2^{t(k-2)} \cdot \frac{w_i^s}{\rho^{2t}}\sigma(\tilde{x})^{s-2t}. \tag{9.15}$$

The above equation gives the bound for contributions of the sample points inside a single leaf node NC_k at any level $k \geq 2$. We use induction to establish that the bound also holds for any *internal* node. Let NC_k be an internal node. Then, by induction we can assume that each of the 27 children of NC_k satisfy Inequality 9.15 with $k = k+1$. Summing over this 27 children and replacing

k with $k+1$ in Inequality 9.15, we get

$$\sum_{p \in NC_k} I_p(x) \leq \lambda \exp^{-2^{k-1}\frac{rw_i}{(1+2r)\rho^2}} \cdot 2^{t(k-1)} \cdot \frac{w_i^s}{\rho^{2t}} \sigma(\tilde{x})^{s-2t}$$
$$\leq \frac{1}{27} \cdot \lambda \exp^{-2^{k-2}\frac{rw_i}{(1+2r)\rho^2}} \cdot 2^{t(k-2)} \cdot \frac{w_i^s}{\rho^{2t}} \sigma(\tilde{x})^{s-2t}.$$

The lemma follows from the fact that 27 NC_2s partition $D_{\frac{\rho}{2}}$. ■

Theorem 9.2. *If $\rho \leq 0.4$, $\varepsilon \leq 0.1$, and $r \geq 5\rho$, then for any $x \in \mathbb{R}^3$*

$$\sum_{p \notin B_{x,rf(\tilde{x})}} I_p(x) \leq C_1 \lambda \cdot \frac{r^2 + r\rho + \rho^2}{\rho^2} \exp^{-\frac{r^2}{(1+2r)\rho^2}} \cdot \frac{r^s}{\rho^{2t}} \sigma(\tilde{x})^{s-2t}$$

where $0 \leq s \leq 2$, $0 \leq t \leq 1$, and $C_1 = 180\sqrt{3}\pi$.

Proof. The space outside $B_{x,rf(\tilde{x})}$ can be decomposed by $(\mathbb{S}_x(w_i, \rho))_{i=0}^{\infty}$ where $w_i = r + i\rho$. Each $\mathbb{S}_x(w_i, \rho)$ can be covered by less than $\frac{36\sqrt{3}\pi(w_i^2 + w_i\rho + \rho^2)}{\rho^2}$ balls of radius $\frac{\rho}{2} f(\tilde{x})$. From Lemma 9.5 the contribution from the sample points inside each of these balls are bounded. Hence,

$$\sum_{p \notin B_{x,rf(\tilde{x})}} I_p(x) = \sum_{i=0}^{\infty} \sum_{p \in \mathbb{S}_x(w_i,\rho)} I_p(x)$$
$$\leq \frac{C_1\lambda}{5} \sum_{i=0}^{\infty} \frac{w_i^2 + w_i\rho + \rho^2}{\rho^2} \exp^{-\frac{rw_i}{(1+2r)\rho^2}} \cdot \frac{w_i^s}{\rho^{2t}} \sigma(\tilde{x})^{s-2t}$$
$$\leq C_1 \lambda \cdot \frac{r^2 + r\rho + \rho^2}{\rho^2} \exp^{-\frac{r^2}{(1+2r)\rho^2}} \cdot \frac{r^s}{\rho^{2t}} \sigma(\tilde{x})^{s-2t}.$$

The last inequality holds because the series is bounded from above by a geometric series with common ratio less than 0.8. ■

9.4 Surface Properties

Although we prove Theorem 9.2 with the hypothesis that $\rho \leq 0.4$ and $\varepsilon \leq 0.1$ which is plausible in practice, our proof for topological guarantees uses the setting $\varepsilon \leq 4 \times 10^{-3}$ and $\rho = \varepsilon$. Also, we assume $\kappa = 5$ in our calculations. The requirement for such small ε is probably an artifact of the proof technique. There is room to improve these constants though the proofs become more complicated (see the discussion at the end of the section). We focus more on demonstrating the ideas behind the proofs rather than tightening the constants. In practice, AMLS surfaces work well on data sets sparser than the one required by theory, see some examples in Section 9.5.

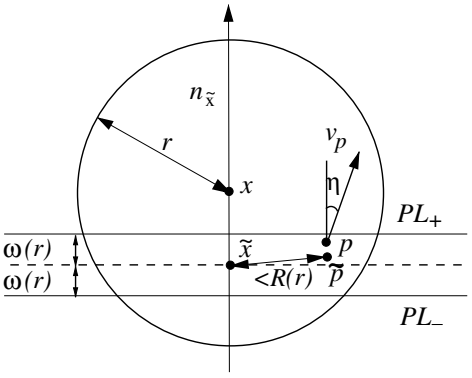

Figure 9.6. All marked distances are in unit of $f(\tilde{x})$. η is the angle between $\mathbf{n}_{\tilde{x}}$ and $\mathbf{v}_p$.

Recall that, for the homeomorphism claim, we only have to show that there exist δ and δ' with $\delta' < \delta < 1$ so that $\mathcal{N}$ has the Hausdorff property for some δ and δ' and the gradient property for δ'. We establish these properties for $\delta = 0.1$ and $\delta' = 0.3\varepsilon$. Then, by definition, $W = \mathcal{N}^{-1}(0) \bigcap 0.1\Sigma$ is the implicit surface of our interest. We establish the Hausdorff property in Lemma 9.7 and the gradient property in Lemma 9.8.

Since function values f and σ are very close to each other, the difference between the values of these two functions will not affect the result of the proof as we already demonstrate in the proof of Lemma 9.5. For the sake of simplicity, we make no difference between the values of these two functions for the proofs in the rest of this section.

9.4.1 Hausdorff Property

In our proof of the Hausdorff property, Lemma 9.4 plays a crucial role. We summarize the statement of the lemma once more here. As Figure 9.6 shows, for a point x on $\Sigma_{+\delta}$ or $\Sigma_{-\delta}$, all sample points inside $B_{x,rf(\tilde{x})}$ are inside a narrow slab bounded by two planes PL_+ and PL_- with $\omega(r)$ distance to $\tilde{x}$ if δ and r are small. In addition, the proof of Lemma 9.4 implies that the distance between $\tilde{x}$ and $\tilde{p}$ is less than $R(r)$ (see Lemma 9.4 for definitions of $R(r)$ and $\omega(r)$). For brevity write $R = R(r)$ and $\omega = \omega(r)$.

The following lemma is used in proving the Hausdorff property. Let $\tau = \frac{\sqrt{2}}{1-\varepsilon}$.

Lemma 9.6. *Let x be a point on $\Sigma_{\pm\delta}$ and p be any sample point inside $B = B_{x,rf(\tilde{x})}$ where $r = \sqrt{2\tau}\delta + 5\rho$. If $0.3\varepsilon \le \delta \le 0.1$ then*

$$(x-p)^T \mathbf{v}_p \ge (0.9\delta - 45\varepsilon^2) f(\tilde{x}) \quad \text{if } x \in \Sigma_{+\delta}$$
$$\le (-0.9\delta + 45\varepsilon^2) f(\tilde{x}) \text{ if } x \in \Sigma_{-\delta}$$

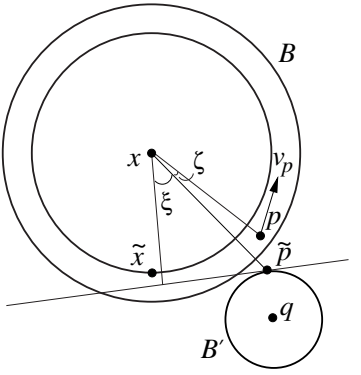

Figure 9.7. Illustration for Lemma 9.6.

Proof. We prove the first half. The second half can be proved similarly. Since $\tilde{x} - \tilde{p} \leq Rf(\tilde{x})$ (Inequality 9.13) we have

$$(1 - R)f(\tilde{x}) \leq f(\tilde{p}) \leq (1 + R)f(\tilde{x}).$$

Under the given values for the parameters, we have $R < 0.18$. In Figure 9.7, B' is the medial ball at $\tilde{p}$ on the side of Σ not containing x. Let q be the center of B'. We have $\|q - \tilde{p}\| \geq f(\tilde{p})$, $\delta f(\tilde{x}) \leq \|x - \tilde{p}\| \leq rf(\tilde{x}) + \varepsilon^2 f(\tilde{p})$, and $\|x - p\| \geq \|x - \tilde{p}\| - \varepsilon^2 f(\tilde{p})$.

Let ξ be the angle between $x\tilde{p}$ and the normal at $\tilde{p}$, and ζ be the angle between xp and $x\tilde{p}$. Hence, the angle between xp and $\mathbf{v}_p$ is less than $\zeta + \xi + \varepsilon$. Since $\|x - \tilde{p}\| \geq \|x - \tilde{x}\| \geq 0.3\varepsilon f(\tilde{x})$ and $\|p - \tilde{p}\| \leq \varepsilon^2 f(\tilde{p})$, we have $\zeta \leq 4\varepsilon$. In addition

$$\|x - q\|^2 = (\|x - \tilde{p}\| \cos\xi + \|q - \tilde{p}\|)^2 + \|x - \tilde{p}\|^2 \sin^2\xi.$$

Since B' is on the side of Σ not containing x, we have $\|x - q\| \geq \|x - \tilde{x}\| + \|q - \tilde{p}\|$. Hence,

$$\cos\xi \geq \frac{2\|x - \tilde{x}\|\|q - \tilde{p}\| + \|x - \tilde{x}\|^2 - \|x - \tilde{p}\|^2}{2\|x - \tilde{p}\|\|q - \tilde{p}\|}.$$

Therefore,

$$\begin{aligned}(x - p)^T \mathbf{v}_p &\geq \|x - p\| \cos(\xi + 5\varepsilon) \\ &\geq (\|x - \tilde{p}\| - (1 + R)\varepsilon^2 f(\tilde{x}))(\cos\xi - 5\varepsilon) \\ &\geq \|x - \tilde{p}\| \cos\xi - 5\varepsilon\|x - \tilde{p}\| - 2\varepsilon^2 f(\tilde{x})\end{aligned}$$

which leads to the first half of the lemma by carefully substituting the inequalities we derived. ■

Lemma 9.7. *For $\rho = \varepsilon$, $\varepsilon \leq 4 \times 10^{-3}$, and $\kappa = 5$*

$$\begin{aligned} \mathcal{N}(x) > 0 \quad & \text{if } x \in (0.1\Sigma \setminus 0.3\varepsilon\Sigma) \cap \Omega_O \\ < 0 \quad & \text{if } x \in (0.1\Sigma \setminus 0.3\varepsilon\Sigma) \cap \Omega_I \ . \end{aligned}$$

Proof. We prove the first half of the lemma. The other half can be proved similarly. Assume $x \in \Sigma_{+\delta}$ for $0.3\varepsilon \leq \delta \leq 0.1$. Let $r = \sqrt{2\tau}\delta + 5\rho$ and $B = B_{x, rf(\tilde{x})}$. For any sample point p inside B, we have from Lemma 9.6

$$((x - p)^T \mathbf{v}_p)\theta_p(x) \geq \theta_p(x) \cdot 0.09\varepsilon f(\tilde{x}) > 0. \tag{9.16}$$

From the sampling condition (i), there exists a sample point p_0 so that $\|\tilde{p}_0 - \tilde{x}\| \leq \varepsilon f(\tilde{x})$ and hence $f(\tilde{p}_0) \geq (1 - \varepsilon) f(\tilde{x})$. In addition we have $\|x - p_0\| \leq (\delta + \varepsilon_1) f(\tilde{x})$ where $\varepsilon_1 = (\varepsilon + \delta + \delta\varepsilon)$ obtained from the Close Sample Lemma 7.1. Thus,

$$\sum_{p \in B}((x - p)^T \mathbf{v}_p)\theta_p(x) > \exp^{-\frac{\tau(\delta+\varepsilon_1)^2}{\rho^2}} \cdot 0.09\varepsilon f(\tilde{x}).$$

Writing

$$\Delta = \frac{\left|\sum_{p \notin B}((x - p)^T \mathbf{v}_p)\theta_p(x)\right|}{\sum_{p \in B}((x - p)^T \mathbf{v}_p)\theta_p(x)}$$

we have

$$\mathcal{N}(x) > \sum_{p \in B}((x - p)^T \mathbf{v}_p)\theta_p(x)(1 - \Delta).$$

If we show $\Delta < 1$, we are done since $\mathcal{N}(x) > 0$ in that case.

Consider the sample points outside B. With $s = 1$ and $t = 0$ in Theorem 9.2 we have

$$\begin{aligned} \left|\sum_{p \notin B}((x - p)^T \mathbf{v}_p)\theta_p(x)\right| &\leq \sum_{p \notin B} \exp^{-\frac{\sqrt{2}\|x-p\|^2}{\rho^2 \sigma(\tilde{p})\sigma(\tilde{x})}} \|x - p\| \\ &\leq C_1\lambda \frac{r^2 + r\rho + \rho^2}{\rho^2} \exp^{-\frac{r^2}{(1+2r)\rho^2}} \cdot r\sigma(\tilde{x}). \end{aligned}$$

Hence,

$$\begin{aligned} \Delta &\leq C_1\lambda \frac{r^2 + r\rho + \rho^2}{\rho^2} \exp^{-\frac{(\sqrt{2\tau}\delta+5\rho)^2}{(1+2r)\rho^2} + \frac{\tau(\delta+\varepsilon_1)^2}{\rho^2}} \cdot \frac{r}{0.09\varepsilon} \\ &\leq C_1\lambda \frac{r^2 + r\rho + \rho^2}{\rho^2} \exp^{-\frac{(\sqrt{2\tau}\delta+5\rho)^2}{2\rho^2} + \frac{\tau(\delta+\varepsilon_1)^2}{\rho^2}} \cdot \frac{r}{0.09\varepsilon} \end{aligned} \tag{9.17}$$

since $(1 + 2r) < 2$. Since the ball $B_{x, \frac{\rho}{2} f(\tilde{x})} = B_{x, \frac{\varepsilon}{2} f(\tilde{x})}$ contains at most 10κ sample points from Lemma 9.3 we have $\lambda \leq 10\kappa \leq 50$. The quantity on the

right of Inequality 9.17 reaches maximum when δ attains its minimum 0.3ε. So, substituting all values we obtain

$$\Delta = \frac{|\sum_{p\notin B}\big((x-p)^T\mathbf{v}_p\big)\theta_p(x)|}{\sum_{p\in B}\big((x-p)^T\mathbf{v}_p\big)\theta_p(x)} < 1$$

as we are supposed to show. ■

9.4.2 Gradient Property

In the following lemma we prove the gradient property of $\mathcal{N}$ for $\delta = 0.3\varepsilon$.

Lemma 9.8. *Let z be any point on Σ, then for any $x \in \ell_{\mathbf{n}_z} \cap 0.3\varepsilon\Sigma$*

$$[\mathbf{n}_z]\mathcal{N}(x) > 0$$

for $\rho = \varepsilon$, $\varepsilon \le 4\times 10^{-3}$, and $\kappa = 5$.

Proof. Recall $\tilde{x} = \nu(x)$ and hence $\sigma(\tilde{x}) = f\circ\nu(x)$. Obviously, since x avoids the medial axis of Σ, $[\mathbf{n}_{\tilde{x}}](f\circ\nu)(x) = 0$. Since $z = \tilde{x}$, we have

$$\begin{aligned}[\mathbf{n}_z]\mathcal{N}(x) &= \sum_{p\in P}[\mathbf{n}_z]((x-p)^T\mathbf{v}_p\theta_p(x))\\ &= \sum_{p\in P}\theta_p(x)\left(\mathbf{n}_{\tilde{x}}^T\mathbf{v}_p - 2\frac{\sqrt{2}(x-p)^T\mathbf{v}_p\cdot(x-p)^T\mathbf{n}_{\tilde{x}}}{\rho^2\sigma(\tilde{p})\sigma(\tilde{x})}\right).\end{aligned}$$

Let

$$r = \sqrt{2\tau(\delta+\varepsilon_1)^2 + 25\rho^2}. \tag{9.18}$$

and $B = B_{x,rf(\tilde{x})}$. For any sample point p inside B, we know it is inside the slab bounded by two planes from Lemma 9.4 as Figure 9.6 shows. In addition we have $f(\tilde{p}) \ge (1-R)f(\tilde{x})$ from Inequality 9.13. We observe from Figure 9.6 that $|(x-p)^T\mathbf{n}_z| \le (\omega+\delta)f(\tilde{x})$ and $|(x-p)^T\mathbf{v}_p| \le (\omega+\delta+r\eta)f(\tilde{x})$. Under the given values for the parameters, we have $r < 5.68\varepsilon$ and $R < 6\varepsilon$. Hence, from Lemma 9.4 $\omega < 20\varepsilon^2$ and $\eta < 0.03$. Using these values we get

$$\theta_p(x)\left(\mathbf{n}_{\tilde{x}}^T\mathbf{v}_p - 2\frac{\sqrt{2}|(x-p)^T\mathbf{v}_p|\cdot|(x-p)^T\mathbf{n}_{\tilde{x}}|}{\rho^2(1-R)f^2(\tilde{x})}\right) \ge 0.4\theta_p(x). \tag{9.19}$$

Hence,

$$[\mathbf{n}_z](((x-p)^T\mathbf{v}_p)\theta_p(x)) \ge 0.4\theta_p(x) > 0.$$

In particular, there exists a sample point p_0 so that $\|\tilde{p}_0 - \tilde{x}\| \le \varepsilon f(\tilde{x})$ and hence $f(\tilde{p}_0) \ge (1-\varepsilon)f(\tilde{x})$. In addition we have $\|x-p_0\| \le (\delta+\varepsilon_1)f(\tilde{x})$ where

$\varepsilon_1 = (\varepsilon + \delta + \delta\varepsilon)$ is obtained from the Close Sample Lemma 7.1. Hence,

$$\sum_{p\in B}[\mathbf{n}_z]((x-p)^T\mathbf{v}_p\theta_p(x)) > 0.4\ \exp^{-\frac{\tau(\delta+\varepsilon_1)^2}{\rho^2}}.$$

Writing

$$\Delta = \frac{\left|\sum_{p\notin B}[\mathbf{n}_z]\big(\big((x-p)^T\mathbf{v}_p\big)\theta_p(x)\big)\right|}{\sum_{p\in B}[\mathbf{n}_z]\big(\big((x-p)^T\mathbf{v}_p\big)\theta_p(x)\big)}$$

we have

$$[\mathbf{n}_z]\mathcal{N}(x) > \sum_{p\in B}[\mathbf{n}_z]((x-p)^T\mathbf{v}_p\theta_p(x))(1-\Delta).$$

If we show $\Delta < 1$ we are done since $[\mathbf{n}_z]\mathcal{N}(x) > 0$ in that case.

Consider the sample points outside B. We have

$$\begin{aligned}
&\left|\sum_{p\notin B}[\mathbf{n}_z]((x-p)^T\mathbf{v}_p\theta_p(x))\right| \\
&= \sum_{p\notin B}\theta_p(x)\left(\mathbf{n}_{\tilde{x}}^T\mathbf{v}_p - 2\frac{\sqrt{2}(x-p)^T\mathbf{v}_p\cdot(x-p)^T\mathbf{n}_{\tilde{x}}}{\rho^2\sigma(\tilde{p})\sigma(\tilde{x})}\right) \\
&\le \sum_{p\notin B}\exp^{-\frac{\sqrt{2}\|x-p\|^2}{\rho^2\sigma(\tilde{p})\sigma(\tilde{x})}}\left(1+2\frac{\sqrt{2}\|x-p\|^2}{\rho^2\sigma(\tilde{p})\sigma(\tilde{x})}\right). \qquad (9.20)
\end{aligned}$$

From Theorem 9.2 the right side in Inequality 9.20 is no more than

$$C_1\lambda\frac{r^2+r\rho+\rho^2}{\rho^2}\cdot\ \exp^{-\frac{r^2}{(1+2r)\rho^2}}\left(1+2\frac{r^2}{\rho^2}\right).$$

Therefore,

$$\Delta < \frac{C_1\lambda}{0.4}\frac{r^2+r\rho+\rho^2}{\rho^2}\cdot\exp^{-\frac{25}{1+2r}}\left(1+2\frac{r^2}{\rho^2}\right)$$

which is less than 1 when r is evaluated for $\rho = \varepsilon \le 4\times10^{-3}$ from relation 9.18 and λ is plugged in from Lemma 9.3. ■

The requirement for small ε is mainly because of the following fact. Our proof requires that Inequalities 9.16 and 9.19 be true for all the sample points inside B. This means all the sample points inside B make positive contribution to the implicit function and its derivative. However, one can relax this requirement by further classifying the sample points inside B and allowing the sample points close to the boundary of B to make negative contributions. Since these sample points have small weights, their contributions do not change the positivity of the entire contribution from the sample points inside B.

We have proved that W and Σ are homeomorphic. It can also be proved that they are isotopic. Since W lives in a small tubular neighborhood of Σ and the segments normal to Σ intersect W in a single point within this tubular neighborhood, one can define an isotopy connecting W and Σ. This construction is exactly the same as the one used to prove that the power crust and the sampled surface are isotopic in the PC-Isotopy Theorem 6.4.

9.5 Algorithm and Implementation

In this section we summarize different steps of the algorithm for reconstructing with AMLS surfaces. We already know that the definition of AMLS involves the local feature sizes of the sampled surface Σ. In absence of Σ one cannot compute $f(\tilde{x})$ and hence $\sigma(\tilde{x})$ for a point x exactly. Due to this difficulty, we describe an implementation that can only approximate the AMLS surface. Recall that each sample point p is assumed to have an associated normal $\mathbf{v}_p$ that approximates the normal at $\tilde{p}$. So, for a sample P without any normal information, the approximation of the AMLS surface also needs to estimate the normals at the sample points.

9.5.1 Normal and Feature Approximation

In Chapter 7, we have already presented the algorithms for the normal and feature approximations from noisy point samples. The routine ApproximateNormal takes P and a threshold τ to decide which Delaunay balls in Del P are big enough to give good approximation of normals.

The normals computed by ApproximateNormal are not consistently oriented. The input points should be equipped with oriented normals for AMLS approximation. We orient the normals by walking over the points and propagating the orientation in the neighborhoods. We compute a minimum spanning tree of the points. It can be shown that any edge in the minimum spanning tree must connect two points p, q that are only $\tilde{O}(\varepsilon)\max\{f(p), f(q)\}$ distance apart. This means the true normals $\mathbf{n}_{\tilde{p}}$ and $\mathbf{n}_{\tilde{q}}$ differ only by a small amount and hence $\mathbf{v}_p$ and $\mathbf{v}_q$ should be similarly oriented. If during the walk we move from p to q where the normal $\mathbf{v}_p$ has been oriented, we orient $\mathbf{v}_q$ as follows. If a normal has not been computed by ApproximateNormal at q, we transport $\mathbf{v}_p$ to q. This means we set $\mathbf{v}_q$ to be parallel to $\mathbf{v}_p$ and orient it the same way as $\mathbf{v}_p$. In case ApproximateNormal has computed a normal at q, we orient $\mathbf{v}_q$ so that $\mathbf{v}_p^T\mathbf{v}_q$ is positive. One can show easily that this procedure orients the normal at any point p so that $\mathbf{v}_p$ and $\mathbf{n}_{\tilde{p}}$ make an angle less than $\frac{\pi}{2}$ thereby ensuring a consistent orientation.

```
OrientNormal(P,τ)
1   ApproximateNormal(P,τ);
2   compute a minimum spanning tree T of P;
3   let r be any point assigned a normal by ApproximateNormal;
4   carry out a depth-first search in T starting at r;
5   let q be a point reached from p by edge pq ∈ T;
6   if q is assigned normal v_q by ApproximateNormal
7     orient v_q so that v_p^T v_q > 0;
8   else
9     v_q = v_p;
10  endif.
```

We use the routine ApproximateFeature from Chapter 7 to approximate the feature sizes. The routine ApproximateFeature takes P and a user parameter k to determine the poles approximating the medial axis by searching the k-nearest neighbors of the sample points. Then, it estimates the local feature size by computing the distances of the sample points to these poles. We use OrientNormal and ApproximateFeature to preprocess P and then apply a projection procedure to move a point in P to the AMLS surface.

9.5.2 Projection

The sample points are moved to the AMLS surface by the Newton projection method. It is an iterative procedure in which we move a point p to a new point p' along $\nabla\mathcal{I}(p)$ where

$$p' = p - \frac{\mathcal{I}(p)}{\|\nabla\mathcal{I}(p)\|^2}\nabla\mathcal{I}(p). \tag{9.21}$$

This iteration continues until the distance between p and p' becomes smaller than a given threshold τ'. To compute $\mathcal{I}(p)$ and $\nabla\mathcal{I}(p)$, one may take the sample points inside the ball with radius a small multiple of the width of the Gaussian weighting function since the sample points outside this ball have little effect on the function. We supply the parameter ρ which appear in the computations of $\mathcal{I}(p)$ and $\nabla\mathcal{I}(p)$. We see in the examples that the Newton iteration for AMLS surface converges quickly and has a big convergent domain in Section 9.6.

Finally, the projected set of points are fed to a reconstruction algorithm, say Cocone, to produce the output. Figure 9.8 shows the results of this algorithm applied on Max-Planck and Bighand point clouds.

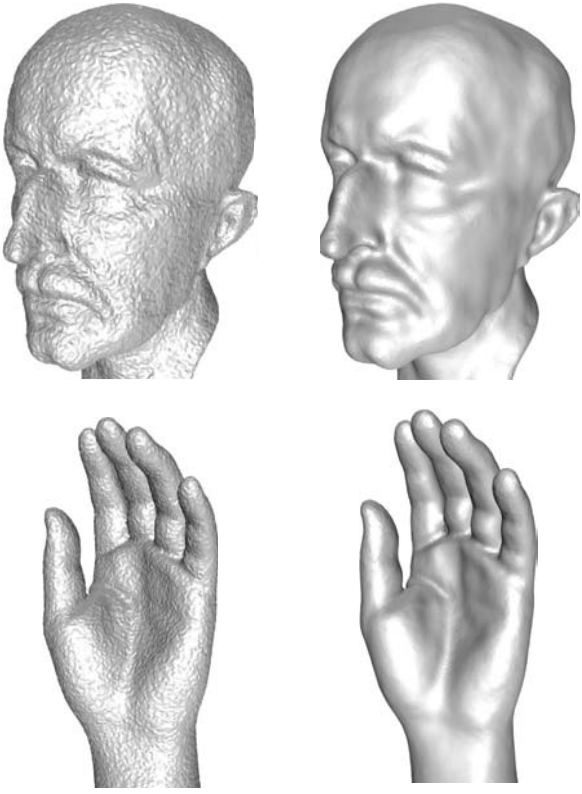

Figure 9.8. Reconstruction results before (left) and after (right) smoothing with AMLS. $\rho = 0.75$ for both models. The reason a bigger ρ is chosen than the one (0.4) we suggest in Section 9.2.1 is that the feature approximation method tends to compute a feature size slightly smaller than the exact one.

AMLS(P,τ,k,τ',ρ)

```
1  OrientNormal(P,τ);
2  ApproximateFeature(P,k);
3  for each p ∈ P do
4     compute p′ by equation 9.21;
5     if ‖p − p′‖ > τ′
6        go to 4 with p := p′;
7  endfor
8  let P′ be the projected point set;
9  Cocone(P′).
```

9.6 Other MLS Surfaces

9.6.1 Projection MLS

There is another implicit surface which is popularly known as an MLS surface in graphics. This surface was originally defined procedurally. Later an implicit formulation was discovered. To differentiate this surface from the one we just described, we call this surface *projection* MLS or PMLS in short.

The PMLS surface is defined as the stationary set of a map $\phi : \mathbb{R}^3 \to \mathbb{R}^3$, that is, the points $x \in \mathbb{R}^3$ with $\phi(x) = x$. The map ϕ at a point $x \in \mathbb{R}^3$ is defined procedurally. Let $\mathcal{E} : \mathbb{R}^3 \times \mathbb{R}^3 \to \mathbb{R}^3$ be the following map. Given a vector $\mathbf{v} \in \mathbb{R}^3$ and a point $y = x + t\mathbf{v}$ for some real $t \in \mathbb{R}$, $\mathcal{E}(y, \mathbf{v})$ is defined to be the sum of the weighted distances of all points in P from a plane with normal $\mathbf{v}$ and the point y. Specifically,

$$\mathcal{E}(y, \mathbf{v}) = \Sigma_{p \in P}((y - p)^T \mathbf{v})^2 \theta_p(y) \tag{9.22}$$

where θ_p is a weighting function. The nearest point to x where $\mathcal{E}$ is minimized over all directions v and all reals t defining y is $\phi(x)$.

This minimization procedure can be decomposed into two optimization steps. The first one finds an optimum direction and the second one uses this optimum direction to find the required minimum. For a point x let $\mathbf{n}(x)$ be the optimum direction found by the first optimization, that is,

$$\mathbf{n}(x) = \arg\min_{\mathbf{v}} \mathcal{E}(y, \mathbf{v}). \tag{9.23}$$

Let $\ell_{\mathbf{n}(x)}$ denote the line of the vector $\mathbf{n}(x)$.

For x let $\mathcal{E}(y, \mathbf{n}(x))$ achieve a local minimum at x_m over the set $y \in \ell_{\mathbf{n}(x)}$. Mathematically, this implies

$$\mathbf{n}(x)^T \left(\frac{\partial \mathcal{E}(y, \mathbf{n}(x))}{\partial y} |_{x_m} \right) = 0. \tag{9.24}$$

The following result is known.

Fact 9.1. *x is a stationary point of ϕ if $x = x_m$.*

From the above results one gets a projection procedure by which points can be projected onto a PMLS surface. Starting from a point x, the local minimum x_m is computed. Then x is replaced with x_m and the iteration continues till the distance between x and x_m drops below a threshold. Notice that the optimization is done over the set $y \in \ell_{\mathbf{n}(x)}$ where $\mathcal{E}$ depends on y. This makes the optimization procedure nonlinear and hence computationally hard.

One can conclude from Equation 9.24 and Fact 9.1 that the set of stationary points is actually the zero-level set of the implicit function

$$\mathcal{J}(x) = \mathbf{n}(x)^T \left(\frac{\partial \mathcal{E}(y, \mathbf{n}(x))}{\partial y} |_x \right).$$

One needs to be a little more careful. Equation 9.24 does not only hold for minima of $\mathcal{E}$ but also for all of its other extrema including the maxima. Therefore, in general, all components of $\mathcal{J}^{-1}(0)$ are not in PMLS surface. The ones where $\mathcal{E}$ reaches local minimum need to be identified for reconstruction purpose. One can verify that when the weighting function θ_p is a Gaussian as in Equation 9.5, the implicit function $\mathcal{J}$ takes the following form:

$$\mathcal{J}(x) = \sum_{p \in P} (x - p)^T \mathbf{n}(x) \left(1 - \left(\frac{(x - p)^T \mathbf{n}(x)}{h} \right)^2 \right) \theta_p(x). \tag{9.25}$$

Notice that, instead of computing $\mathbf{n}(x)$ as in Equation 9.23, one may assume that the input points are equipped with some normals from which a normal field $\mathbf{n} : \mathbb{R}^3 \to \mathbb{R}^3$ can be derived, say by a simple linear interpolation.

9.6.2 Variation

The expression for $\mathcal{J}$ is a little cumbersome for projecting points as it leads to nonlinear optimizations. It can be simplified if we modify $\mathcal{E}$ slightly. Observe that the weighting function θ_p varies with y in the expression for $\mathcal{E}$ in Equation 9.22. Instead, we can vary θ_p with x. Then, we get a slightly different implicit function $\mathcal{G}$ than $\mathcal{J}$:

$$\mathcal{G}(x) = \sum_{p \in P} [(x - p)^T \mathbf{n}(x)] \theta_p(x). \tag{9.26}$$

The surface given by $\mathcal{G}^{-1}(0)$ is a variation of the PMLS surface and hence we call it VMLS surface. An advantage of the VMLS surface is that, unlike the standard PMLS surfaces, its inherent projection procedure does not require any nonlinear optimization, which makes the algorithm faster, more stable and easier to implement.

9.6.3 Computational Issues

We have chosen $\mathcal{I}$ instead of $\mathcal{N}$ to define the AMLS surface though the topological and geometric guarantees can be worked out with both. The reason is mainly a practical consideration. Newton projections have larger convergent domain for $\mathcal{I}$ than $\mathcal{N}$. Figure 9.9 illustrates this fact.

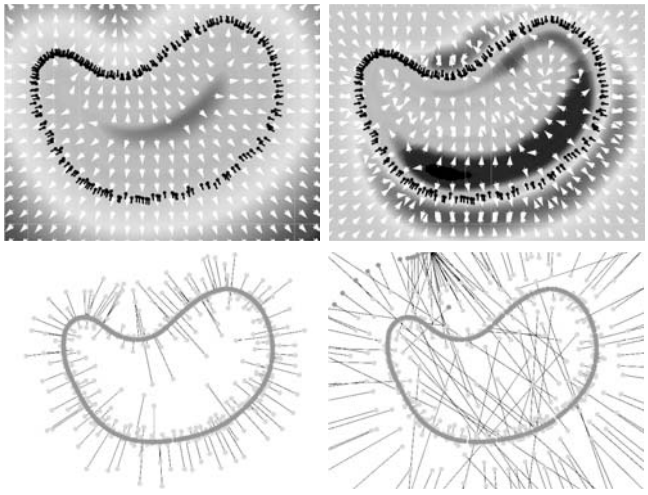

Figure 9.9. The left and right columns show the result of NP on $\mathcal{I}$ and $\mathcal{N}$ respectively. The top row shows the function values and the gradient field. The darker the shade, the higher the absolute value; it is negative inside and positive outside. In the bottom, the lines connect input gray points to their corresponding stationary points of NP.

Advantages of Newton Projections

Although the projection procedure of VMLS surfaces is more efficient than the PMLS surfaces, it turns out that the Newton projections are even better. The VMLS projection can be described as follows. Project x along $\mathbf{n}(x)$ to a new position

$$x' = x - \frac{\mathcal{G}(x)}{\sum_{p \in P} \theta_p(x)} \mathbf{n}(x) \tag{9.27}$$

and iterate until a stationary point is reached. Due to its linear nature we refer to this projection as Linear Projection or LP in short. The Newton projection for AMLS surfaces is referred to as NP in short. We argue that NP is better than LP in two respects: convergence rate and timing. As Table 9.1 shows, NP, in general, uses less iterations to project a point onto the implicit surface. This is not surprising as $\nabla \mathcal{I}(x)$ with x close to the implicit surface can estimate the normal more accurately at its closest point on the implicit surface. In addition, one has to compute $\mathbf{n}(x)$ before evaluating $\mathcal{G}(x)$. Hence to compute the new position using LP, one has to iterate twice over its neighboring points which makes LP slower than NP even in each iteration.

Table 9.1. *Time data for NP and LP. |P| is the number of points in the point cloud.*

Model	|P|	Method	#nb	#iter	Time
Max-planck	49137	NP	1000	3.1	94
		LP	1108	7.2	310
Bighand	38214	NP	1392	3.2	109
		LP	1527	8.6	400

#iter is the number of iterations in the average sense, i.e., we add up the number of iterations used to project all the input points and divide it by |P| to get #iter. Similarly, #nb is the average number of points considered as neighbors. $\tau' = 10^{-25}$ for these experiments. Times (second) are for projecting all the input points (PC with a 2.8 GHz P4 CPU and 1 GB RAM).

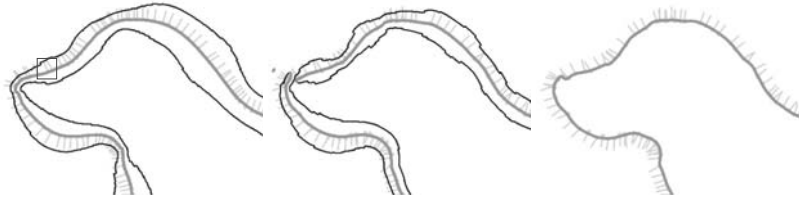

Figure 9.10. The leftmost and the middle pictures show zero-level sets of the standard PMLS under two different noise levels. The noise level in the middle is higher. Thicker curves represent the zero-level set $\mathcal{J}^{-1}(0)$ where $\mathcal{E}$ reaches minima while the thinner curves are zero-level sets where the energy function reaches maxima. The rightmost picture shows the zero-level set $\mathcal{I}^{-1}(0)$ under the same noise level as in the middle picture.

Zero-Level Sets

In the definition of PMLS, the actual PMLS surface is only a subset of the zero-level set $\mathcal{J}^{-1}(0)$ where the energy function $\mathcal{E}$ reaches a minimum along the normal direction. As one can deduce from Equation 9.25, there are two other layers of zero-level sets of the implicit function $\mathcal{J}$ on both sides of the PMLS surface, where the energy function $\mathcal{E}$ reaches the local maximum; see the left most picture in Figure 9.10. We refer to these two layers as *maxima layers*. The distance between these layers could be extremely small at places where either the local feature size is small or the noise level is high or both. In that case, computations on the PMLS surface become difficult.

First of all, many existing implicit surface techniques such as raytracing and polygonizing become hard to apply on the PMLS surface since one needs to distinguish different zero-level sets. When the maxima layers come close to the

true PMLS surface, the marching step in a raytracer and the size of the cubes in a polygonizer may become impractically small.

Second, the projection procedure for the PMLS surface requires a nonlinear optimization, specifically an one-dimensional minimization. The one-dimensional minimization algorithms usually begin with an interval known to contain a minimum guess m such that the function value at m must be less than the function values at the ends of the interval. Finding such a minimum guess m could be hard if the two maxima layers come close.

Third, the PMLS surface is more sensitive to the noise. When the noise level for position or normal or both increases, the three layers of the zero-level sets (one for minima and two for maxima) could easily interfere with each other. In the middle picture of Figure 9.10, the zero-level set for minima gets merged with those for maxima. As a result, the PMLS could give an implicit surface with holes or disconnectness. However, under the same level of noise, the AMLS still gives the proper implicit surface, see the rightmost picture in Figure 9.10.

9.7 Voronoi-Based Implicit Surface

There is a Voronoi diagram-based implicit surface that can be used for surface reconstruction. This method can also be proved to have output guarantees using the ε-sampling theory. We will briefly describe the function definition but will skip the proof of guarantees.

Given an input point set $P \subset \mathbb{R}^3$, the *natural neighbors* $N_{x,P}$ of a point $x \in \mathbb{R}^3$ are the Delaunay neighbors of x in $\mathrm{Del}(P \cup x)$. Letting $V(x)$ denote the Voronoi cell of x in $V_{P\cup x}$, this means

$$N_{x,P} = \{p \in P \mid V(x) \cap V_p \neq \emptyset\}.$$

Let $A(x, p)$ denote the volume stolen by x from V_p, that is,

$$A(x, p) = V(x) \cap V_p.$$

The natural coordinate associated with a point p is a continuous function $\lambda_p : \mathbb{R}^3 \to \mathbb{R}$ where

$$\lambda_p(x) = \frac{A(x, p)}{\Sigma_{q\in P} A(x, q)}.$$

Some of the interesting properties of λ_p are that it is continuously differentiable everywhere except at p and any point $x \in \mathbb{R}^3$ is a convex combination of its natural neighbors, that is, $\Sigma_{p\in N_{x,p}} \lambda_p(x)p = x$. Assume that each point p is equipped with a unit normal $\mathbf{n}_p$ which can either be computed via pole vectors, or be part of the input. A distance function $h_p : \mathbb{R}^3 \to \mathbb{R}$ for each point p

is defined as $h_p(x) = (p - x)^T \mathbf{n}_p$. A global distance function $h : \mathbb{R}^3 \to \mathbb{R}$ is defined by interpolating these local distance functions with natural coordinates. Specifically,

$$h(x) = \Sigma_{p \in P} \lambda_p(x) h_p(x).$$

One difficulty of working with such h is that it is not continuously differentiable everywhere as λ_p is not. To overcome this difficulty one may choose a smooth function arbitrarily close to λ_p and make h smooth everywhere. By definition, $h(x)$ locally approximates the signed distance from the tangent plane at each point $p \in P$ and, in particular, $h(p) = 0$.

When h is made continuously differentiable, $\hat{\Sigma} = h^{-1}(0)$ is a smooth surface unless 0 is a critical value. A discrete approximation of $\hat{\Sigma}$ can be computed from the restricted Delaunay triangulation $\text{Del } P|_{\hat{\Sigma}}$. All Voronoi edges that intersect $\hat{\Sigma}$ are computed via the sign of h at their two endpoints. The dual Delaunay triangles of these Voronoi edges constitute a piecewise linear approximation of $\hat{\Sigma}$. If the input sample P is a ε-sample of a surface Σ for sufficiently small ε, then it can be shown that $\hat{\Sigma}$ is geometrically close and is also topologically equivalent to Σ.

9.8 Notes and Exercises

The definition of MLS surfaces as described in Section 9.2 is taken from Shen, O'Brien, and Shewchuk [77]. The adaptive MLS surface definition and its proofs of guarantees are taken from Dey and Sun [40]. Historically, these definitions were proposed later than the PMLS definition. Levin [65] pioneered the PMLS definition. This definition and its variants such as the VMLS are popularly known as MLS surfaces in graphics. Alexa et al. [1] brought the PMLS surface to the attention of the graphics community in the context of surface reconstruction. Later, it was used for different modeling applications [75]. Zwicker, Pauly, Knoll, and Gross [83] implemented the VMLS definition in a modeling software called Pointshop 3D. The understanding of the PMLS surfaces became much more clear after the work of Amenta and Kil [8] who explained its relation to extremal surfaces and gave its implicit form.

Theoretical guarantees about the MLS surfaces in terms of sampling density were not proved until the work of Kolluri [63]. He showed that the MLS surface given by Equation 9.4 has same topology and approximate geometry of the sampled surface under a uniform sampling condition. Subsequently Dey, Goswami, and Sun [35] proved similar guarantees about the PMLS surface. Following these developments Dey and Sun [40] proposed the AMLS definition

and proved geometric and topological guarantees using an adaptive sampling condition.

The natural neighbor-based implicit surface described in Section 9.7 was proposed by Boissonnat and Cazals [16]. The proof of geometric and topological guarantees for this surface is given for noise-free dense samples.

Other than MLS and natural neighbor surfaces, a few other implicit surfaces have been proposed for smooth surface reconstruction. The radial basis function of Carr et al. [18] and the multilevel partition of unity of Ohtake et al. [73] are examples of such surfaces, to name a few. Theoretical guarantees about these surfaces have not been shown.

Exercises

1. In Equation 9.3, we could take $\phi_p = 0$ in anticipation that $I^{-1}(0)$ fits the points in the input point sample P. What is the difficulty one faces with this choice? How can it be overcome?
2. Recall the definition of $\lambda(\rho)$ in Section 9.3.1. Prove that there is a constant c so that $\lambda(\rho) \leq \frac{c\rho^3\kappa}{\varepsilon^3}$ where ρ and ε are sufficiently small.

3^h. We assume P to be a $(\varepsilon, \varepsilon^2, -)$-sample to prove that the AMLS surface is isotopic to Σ. Show the same when P is a $(\varepsilon, \varepsilon, -)$-sample.

4. Prove Inequality 9.13.
5. Consider the minimum spanning tree T of a $(\varepsilon, \varepsilon^2, -)$-sample. Prove that for any edge $pq \in T$, the angle $\angle(\mathbf{n}_{\tilde{p}}, \mathbf{n}_{\tilde{q}})$ is $\tilde{O}(\varepsilon)$.

6^h. Prove that the projection method for PMLS converges [35].

7. Prove Fact 9.1.
8. Improve the bound on $\|\tilde{x} - \tilde{p}\|$ in the proof of Lemma 9.4. Specifically, show that

$$\|\tilde{x} - \tilde{p}\| \leq \sqrt{\frac{\|x - \tilde{p}\|^2 - (\delta f(\tilde{x}))^2}{1 - \delta f(\tilde{x})/\gamma}}$$

from which derive improved bounds on $R(r)$ and $\omega(r)$.

9^h. Carry out the entire proof of the homeomorphism between Σ and the AMLS surface with an improved ε, say $\varepsilon < 0.05$.

10^o. Prove that the Newton projection for AMLS surfaces converges.